JACS
JOURNAL OF THE AMERICAN CHEMICAL SOCIETY
pubs.acs.org/JACS
Article

Thermolabile Cross-Linkers for Templating Precise Multicomponent Metal–Organic Framework Pores

Jackson Geary, Andy H. Wong, and Dianne J. Xiao*

Cite This: J. Am. Chem. Soc. 2021, 143, 10317–10323
Read Online

ABSTRACT: While a number of approaches toward multicomponent metal–organic frameworks have been reported, new strategies affording greater structural versatility and molecular precision are needed to replicate the sophisticated active sites found in enzymes. Here, we outline a general method for templating functional groups within framework pores using thermolabile ligand cross-linkers. We show that tertiary ester-based cross-linkers can be used to install well-defined carboxylic acid pairs at precise relative distances and orientations. The tertiary ester linkages remain intact during framework formation but are readily cleaved to reveal free carboxylic acids upon microwave heating. Successful cross-linker synthesis, framework incorporation, and thermolysis is demonstrated using the mesoporous, terphenyl expanded analogues of MOF-74. When short cross-linkers are used, modeling studies show that the carboxylic acids are installed in a single configuration down the pore channels, spaced ~7 Å apart. These precisely positioned acid pairs can be used as synthetic handles to build up more complex cooperative active sites.

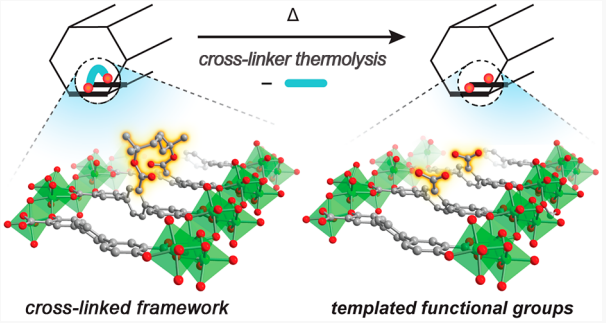

INTRODUCTION

In enzymes, multiple primary and secondary coordination sphere elements work in concert to lower activation barriers and promote catalysis.[1−7] By controlling the spatial arrangement of amino acids and their corresponding side chains, enzymes can direct the self-assembly of complex metal cofactors,[8,9] promote a single reaction outcome over many competing pathways,[2,7] and enhance reaction rates by up to 10^{19}-fold.[2,10]

Crystalline porous materials such as metal–organic frameworks (MOFs) provide an exciting opportunity to explore these bioinspired design principles in the solid state.[11] In theory, many different functional groups, comparable to that of enzymes, can be simultaneously incorporated within MOF pores. In practice, however, current methods still lack the structural versatility and molecular precision needed to replicate biological active sites. Two common strategies toward mixed-ligand MOFs are briefly summarized below. The first is the multivariate approach, where two or more geometrically similar ligands are directly combined to form mixed-ligand frameworks.[12] Multivariate frameworks are distinguished by high chemical and structural diversity but low precision, as the location of functional groups is largely random.[13] On the other end of the spectrum, frameworks composed of two or more geometrically distinct ligands can be used to generate precise pores where functional group positions are crystallographically resolvable. Although creative one-pot[14−17] and sequential ligand installation strategies[18−21] have greatly expanded the scope of frameworks amenable to this strategy, this method is inherently limited to a small subset of MOF structures and ligand geometries.

A less explored but potentially more versatile route toward multicomponent metal–organic frameworks relies on molecular templating, also known as molecular imprinting (Figure 1a). This approach has a rich history in polymer and silica-based materials.[22−24] Small molecules that interact strongly with polymer or silica precursors template the formation of pores with highly complementary surface chemistry, size, and shape. The small molecule templates feature reversible covalent or noncovalent linkages that enable postsynthetic removal. Extending such strategies from amorphous polymer or silica hosts to a crystalline porous framework could be an exceptionally powerful means of generating sophisticated, bioinspired active sites.

The first demonstration of molecular imprinting in MOFs, specifically ZIF-8, was recently reported by Zhou and coworkers.[25] Pairs of imidazole ligands were tethered by imine-based cross-linkers that, upon hydrolysis, revealed templated aldehyde groups. Because the imines readily decomposed during MOF synthesis, the cross-linked ligands could only be

Received: April 16, 2021
Published: June 29, 2021

https://doi.org/10.1021/jacs.1c04030
J. Am. Chem. Soc. 2021, 143, 10317–10323

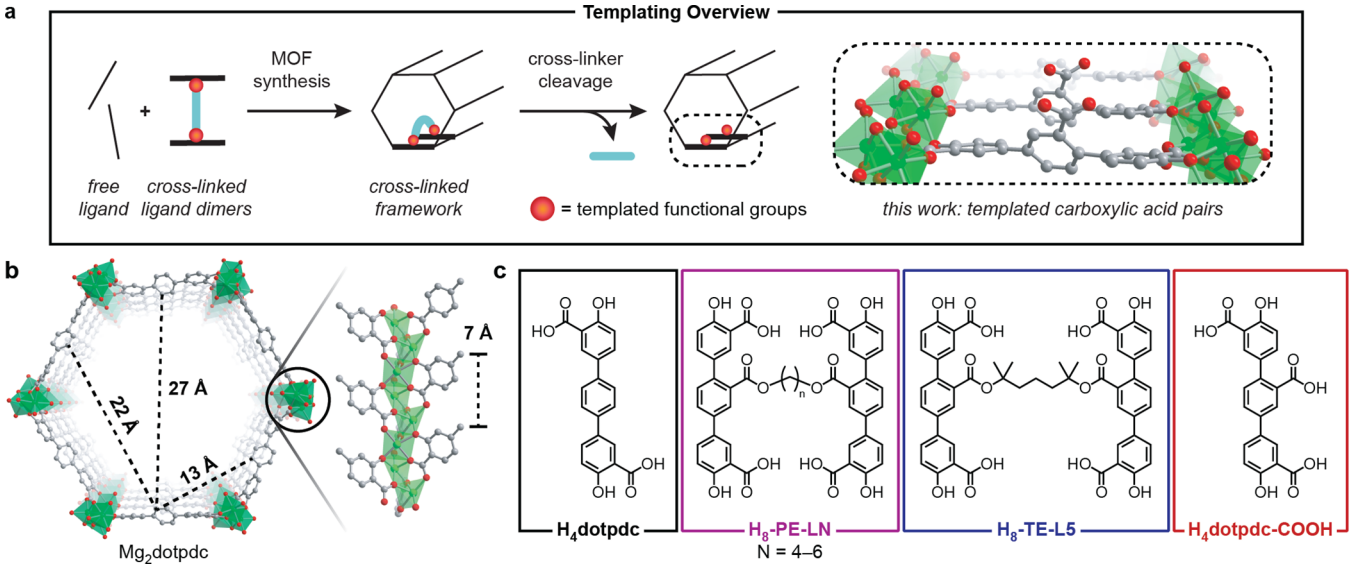

Figure 1. (a) Overview of the templating strategy reported in this work, which relies on the use of cleavable covalent cross-linkers to template the formation of well-defined functional group pairs. This work specifically focuses on the use of ester-based cross-linkers to template carboxylic acids. (b) Structure of Mg_2dotpdc, an expanded MOF-74 analogue, with four distinct interligand distances highlighted. (c) Structures and abbreviations of ligands and cross-linked ligand dimers used in this work.

installed via mild postsynthetic ligand exchange methods. This may limit the scope of imine-based cross-linkers, as not all frameworks undergo facile ligand exchange. Furthermore, from a catalysis viewpoint, the small pore apertures (~3.4 Å) of ZIF-8 greatly restrict the types of active sites and substrates that can be further investigated.[26]

To address these concerns, we sought to design a more chemically stable cross-linker that not only tolerates standard MOF synthesis conditions but also could be adapted to mesoporous (2–50 nm) frameworks. Here, we report the construction of thermolabile, tertiary ester-based cross-linkers that template synthetically versatile carboxylic acid pairs. The ester linkages remain intact during framework formation but are readily thermolyzed into carboxylic acids upon microwave heating. Successful cross-linker synthesis, framework incorporation, and thermolysis are demonstrated using the mesoporous, terphenyl expanded analogues of MOF-74.[27,28] When short pentyl cross-linkers are used, modeling studies suggest that the acid pairs are installed in a single configuration down the pore channels, spaced ~7 Å apart.

RESULTS AND DISCUSSION

Framework Selection and General Templating Strategy. At the outset, an important goal of this work was to extend molecular templating strategies to a mesoporous metal–organic framework, as large pores will be critical for future reactivity studies and catalyst development. Therefore, we selected the MOF-74 archetype (also known as M_2dobdc) for our initial studies,[29] as expanded MOF-74 structures with pore diameters approaching 100 Å have been reported.[27] We have focused on the magnesium-based, terphenyl expanded analogue Mg_2dotpdc (dotpdc^{4-} = 4,4″-dioxido-[1,1′:4′,1″-terphenyl]-3,3″-dicarboxylate), which is highly amenable to ligand functionalization and postsynthetic chemistry.[28,30,31]

The structure of Mg_2dotpdc, modeled in Materials Studio, is illustrated in Figure 1b. Extended, terphenylene-based organic ligands bridge rodlike metal oxide chains to form one-dimensional, hexagonal pores with a diameter of ~27 Å. Four distinct interligand distances are highlighted in Figure 1b: the distance across the hexagonal channel (27 Å), between adjacent hexagonal edges (13 Å) and next-nearest neighbor edges (22 Å), and finally down the pore channels (7 Å). We hypothesized that, by controlling the length and geometry of our ligand cross-linker, we should be able to force functional group pairs to adopt one out of these four relative orientations. A short cross-linker of <10 Å, for example, should tether functional groups pairwise down the pore channels (Figure 1a). Postsynthetic cross-linker cleavage would reveal two functional groups spaced just ~7 Å apart. This strategy would be especially powerful at low functional group concentrations, where all existing methods, such as the standard multivariate approach, would lead to randomly diluted spatial distributions.

Cross-Linker Design. Pioneering studies by the Cohen group have shown that MOFs can be synthesized from chemically cross-linked ligand dimers,[32] trimers,[33] and even polymers,[34] provided that the length and geometry of the covalent tethers are carefully selected. Although a number of cross-linked and "polyMOF" frameworks have been reported for the MOF-5 and UiO-66 families,[32–38] similar studies have not been performed for the MOF-74 structure type. Furthermore, all previous cross-linkers have employed strong amide or ether-based linkages. Cleavage and removal of these cross-linkers has not been previously demonstrated.

In an effort to develop a cleavable cross-linker design viable across a range of MOFs, we sought a structural motif that possessed both high geometric tunability and controllable chemical stability. To that end, ester-based cross-linkers were selected (Figure 1c). Diesters are readily synthesized from carboxylic acids and diols, a number of which are commercially available. Furthermore, the chemical stability of esters is highly dependent on its structure. Primary esters are typically hydrolyzed under basic conditions, while tertiary esters are acid labile and susceptible to thermolysis at elevated temperatures.[39–41] Postsynthetic thermolysis is particularly attractive, given the relatively high thermal stabilities of many metal–organic frameworks (T_d ~ 300 °C or above).[42]

https://doi.org/10.1021/jacs.1c04030
J. Am. Chem. Soc. 2021, 143, 10317–10323

The primary and tertiary ester-based cross-linked ligand dimers outlined in Figure 1c were synthesized from 2,5-dibromobenzoic acid and the corresponding aliphatic diol over three steps in excellent overall yields (55−80%, see the Supporting Information for synthetic details). For this study, we specifically chose short cross-linkers that can span only the smallest interligand distance (~7 Å down the pore channels, see Figure 1b). The resulting dimers are abbreviated H_8-PE-LN and H_8-TE-LN, where PE and TE stand for primary and tertiary ester, respectively, and N refers to the number of methylene units in the alkyl chain (Figure 1c).

Synthesis of Cross-Linked Frameworks. With our ligand dimers in hand, we first tested whether the primary ester-based variants, H_8-PE-LN (N = 4, 5, and 6), could be successfully incorporated into Mg_2dotpdc. These dimers were relatively straightforward to synthesize, as all primary aliphatic diols were commercially available. We have abbreviated all cross-linked frameworks as Mg_2dotpdc-(PE/TE)-LN-R%, where R% indicates the percentage of cross-linked dotpdc^{4-} relative to the total amount of dotpdc^{4-} in the framework.

All attempts to synthesize the expanded MOF-74 structure with mixtures of H_4dotpdc and H_8-PE-L4 led to the formation of undesired phases or poorly crystalline material (Figure S1). From these results, we concluded that a butyl chain is too short to bridge the 7 Å distance between neighboring ligands down the pore walls.

In contrast, when the pentyl cross-linker H_8-PE-L5 was combined with H_4dotpdc and $Mg(NO_3)_2{\cdot}6H_2O$, a clean powder X-ray diffraction (PXRD) pattern matching the parent Mg_2dotpdc framework was obtained. Rigorous washing of the cross-linked materials followed by digestion and ^{1}H NMR analysis confirmed that the amount of cross-linked dotpdc^{4-} incorporated closely matches the amount predicted based on the initial ratio of H_4dotpdc to H_8-PE-L5 (Table S1, Figures S2−S6). Infrared spectroscopy of the ester cross-linked frameworks revealed the growth of a new peak at 1695 cm^{-1}, consistent with an ester carbonyl stretch (Figure S7). Excellent phase purity is maintained, and no peak broadening is observed even at 100% cross-linker incorporation (Figure 2 and Table S4), highlighting how well the length of the pentyl unit matches the geometry of framework. Interestingly, the longer cross-linker H_8-PE-L6 was also readily accommodated in the MOF-74 structure type (Figure S8). For simplicity, the remainder of this study will focus on H_8-PE-L5, as short cross-linker lengths minimize the number of possible ligand configurations within the framework.

The chemically cross-linked Mg_2dotpdc frameworks are permanently porous and display high Brunauer−Emmett−Teller (BET) and Langmuir surface areas (Figure 2, Table 1). For example, Mg_2dotpdc-PE-L5-19% displays BET and Langmuir surface areas of 2700 and 4920 m^2/g, respectively. These values are only slightly lower than those of the parent Mg_2dotpdc framework (Table 1), providing strong evidence that the integrity of the framework is not compromised by cross-linker incorporation and that no dangling or unincorporated ligands are trapped in the pores. Lower surface areas were observed at higher cross-linker concentrations, consistent with the additional mass and volume present inside the pore channels.

After identifying the pentyl unit as the minimum cross-linker length, we next investigated the structurally related tertiary ester-based dimer, H_8-TE-L5. Developing solvothermal conditions compatible with tertiary esters proved more challenging. Under the standard MOF-74 synthesis conditions (120 °C, 16 h), roughly 20% of the H_2-TE-L5 dimer decomposed to form 2 equiv of monomeric ligand containing a free carboxylic acid, H_4dotpdc-COOH (Figure S9). Inadvertent cross-linker cleavage is likely facilitated by the mild acidity of the initial reaction mixture, the elevated temperature, and the prolonged reaction time. Fortunately, shortening the synthesis to 3 h eliminated any observable cross-linker decomposition.

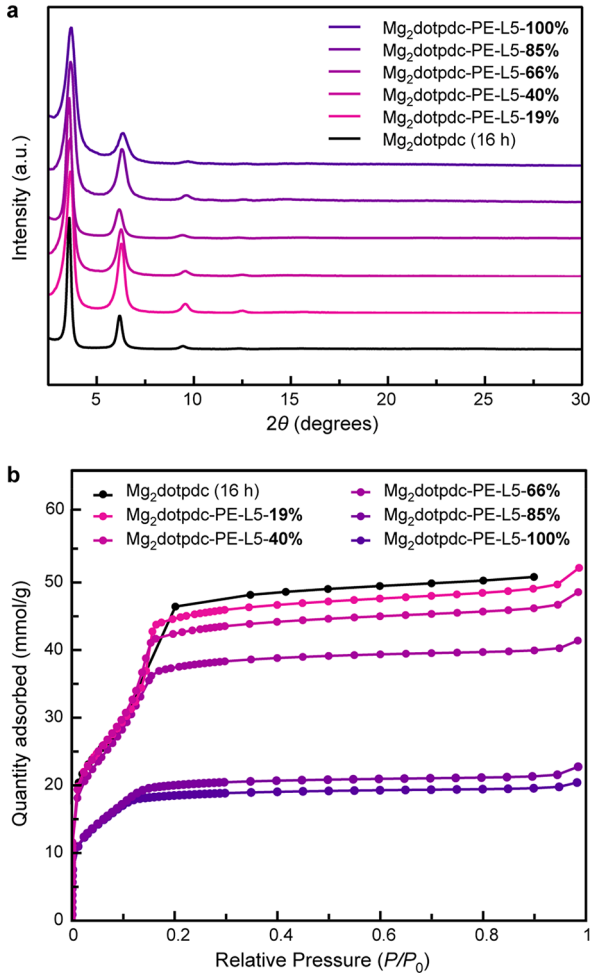

Figure 2. Characterization of primary ester cross-linked Mg_2dotpdc frameworks: (a) PXRD patterns and (b) surface areas of Mg_2dotpdc (16 h) and Mg_2dopdc-PE-L5-R% (R = 19−100%).

Table 1. BET and Langmuir Surface Areas of Mg_2dotpdc, Primary Ester Cross-Linked Mg_2dotpdc-PE-L5-R%, and Tertiary Ester Cross-Linked Mg_2dotpdc-TE-L5-R%

sample	SA_{BET} (m^2/g)	$SA_{Langmuir}$ (m^2/g)
Mg_2dotpdc (16 h)[a]	2700	5120
Mg_2dotpdc (3 h)[a]	2700	4700
Mg_2dotpdc-PE-L5-19%[a]	2700	4920
Mg_2dotpdc-PE-L5-40%[a]	2740	4620
Mg_2dotpdc-PE-L5-66%[a]	2550	3970
Mg_2dotpdc-PE-L5-85%[a]	1630	2150
Mg_2dotpdc-PE-L5-100%[a]	1580	1950
Mg_2dotpdc-TE-L5-23%[b]	2290	3660
Mg_2dotpdc-TE-L5-50%[b]	2250	3300

[a]Samples were activated at 150 °C. [b]All Mg_2dotpdc-TE-L5-R% samples were activated at RT.

https://doi.org/10.1021/jacs.1c04030
J. Am. Chem. Soc. 2021, 143, 10317−10323

Although these short reaction times led to slightly broadened diffraction peaks (Figure S10), similar surface areas were obtained for the parent Mg_2dotpdc framework synthesized at 3 and 16 h (Table 1).

Like their primary ester analogues, the cross-linked frameworks Mg_2dotpdc-TE-L5-R% (R = 23, 50%) display relatively high BET surface areas of ~2300 m^2/g (Table 1). To avoid any cross-linker thermolysis, sample activation was carried out at room temperature. As these mild conditions are not sufficient to remove solvent bound to the Mg^{2+} sites present in the framework, lower surface areas relative to the primary ester analogues were observed. With a 3 h reaction time, slightly greater amounts of cross-linked dotpdc^{4-} are incorporated than expected (e.g., 18% predicted vs 23% observed, see Table S1 and Figures S11–S12), perhaps indicating a small kinetic preference for the cross-linked ligands owing to its templated geometry and higher number of coordination sites.

Modeling Studies. Based on simple geometric considerations, the pentyl cross-linker can adopt one of two configurations within the framework, which we have illustrated in Figure 3. In both structures, labeled "symmetric" and "offset," the cross-linker bridges adjacent ligands down the pore channels. However, they differ in the way the esters are attached to the central phenyl rings. To probe which orientation of the ligand dimer TE-L5^{8-} is energetically preferred, we first optimized the extended structure of Mg_2dotpdc using the Forcite module in Materials Studio. This structure was then truncated to two neighboring ligands and partially frozen such that only the central phenyl rings could freely move, mimicking the geometric restrictions of the MOF lattice. A bridging cross-linker was added, and the geometries of the cross-linker and central phenyl ring were optimized using density functional calculations at the B3LYP/6-311+G(d,p)//B3LYP/6-31+G(d) level of theory. These calculations suggest a strong energetic preference for the symmetric configuration by over 11 kcal/mol (Table S5). As 1.36 kcal/mol corresponds to a 10-fold shift in equilibrium constant, we hypothesize that this configuration is the predominant structure found in the framework.

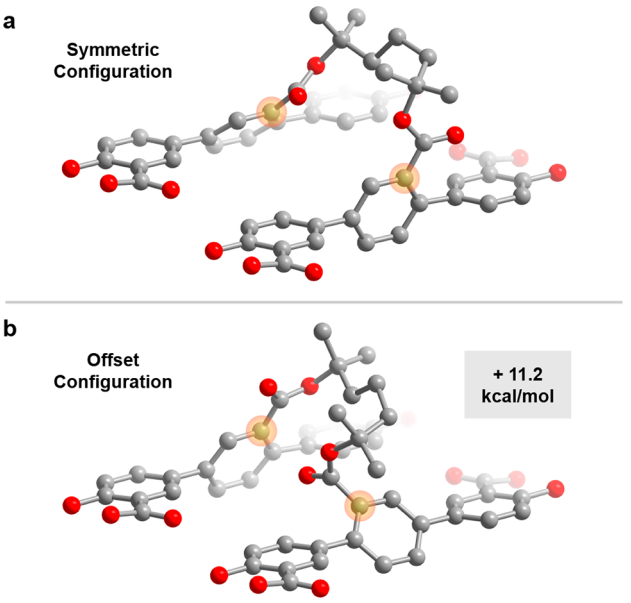

Figure 3. Modeling studies. Truncated structures show the two distinct configurations the cross-linker can adopt down the pore channels, labeled as (a) "symmetric" and (b) "offset." DFT calculations show that the symmetric configuration is more stable by 11.2 kcal/mol.

Cross-Linker Thermolysis. With the successful incorporation of cross-linked ligand dimers firmly established, we finally turned to the last step in our overall templating scheme: postsynthetic cross-linker cleavage. Tertiary esters are known to decompose at elevated temperatures into free carboxylic acids and the corresponding alkenes (Figure 4a).[39−41] While

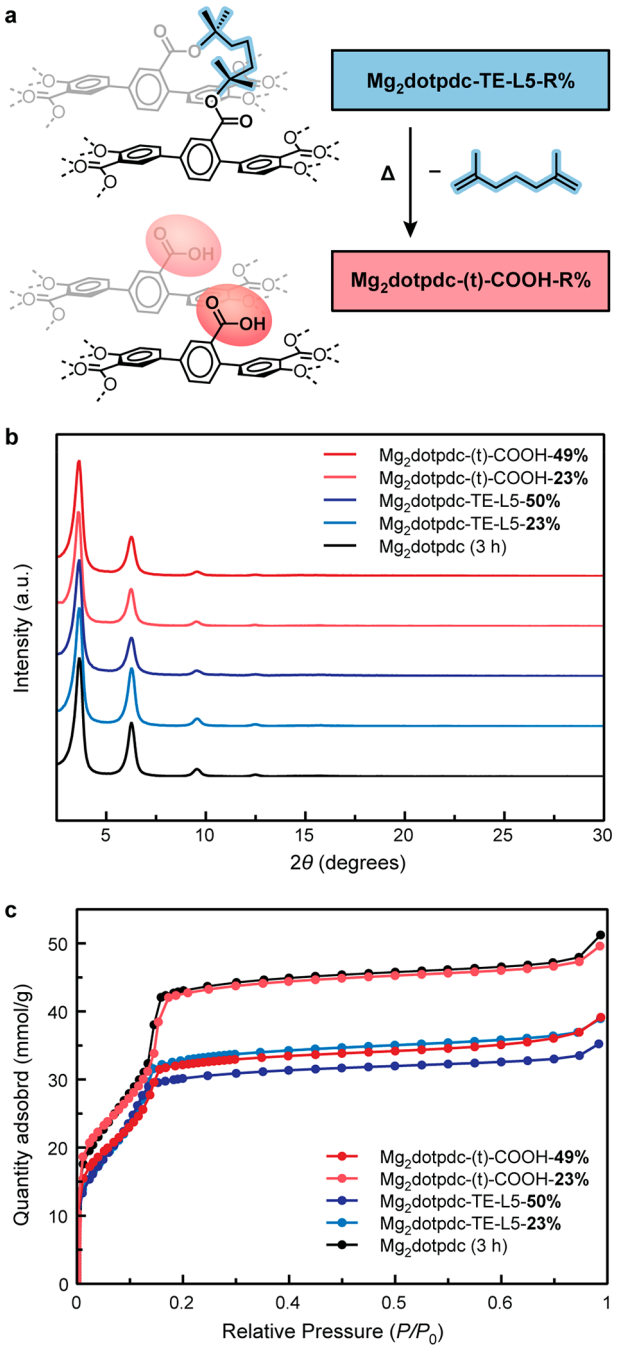

Figure 4. Characterization of tertiary ester cross-linked Mg_2dotpdc frameworks before and after thermolysis. (a) General thermolysis reaction scheme. (b) PXRD patterns and (c) surface areas of Mg_2dotpdc (3 h), cross-linked Mg_2dotpdc-TE-L5-R%, and thermolyzed Mg_2dotpdc-(t)-COOH-R% (R = 23–50%).

https://doi.org/10.1021/jacs.1c04030
J. Am. Chem. Soc. 2021, 143, 10317−10323

this specific reaction has never been demonstrated in a MOF, the analogous thermolysis of tertiary carbamates is well-established,[43,44] and we anticipated that similar conditions could be used.

We adapted a procedure previously reported by Yaghi and co-workers to cleave *tert*-butyl carbamates into free amines, which employed microwave heating at 230 °C for 10 min in a solvent mixture of 2-ethyl-1hexanol, ethylene glycol, and water.[45] We reduced the heating time and eliminated water out of an abundance of caution for the hydrolytic stability of the framework. Excitingly, using this modified procedure, we obtained nearly quantitative conversion (98−99%) of Mg_2dotpdc-TE-L5-R% to Mg_2dotpdc-(t)-COOH-R% (Figures S13 and S14). Note that the (t) denotes the templated, pairwise nature of the carboxylic acids. Importantly, the amount of H_4dotpdc-COOH observed by ^{1}H NMR following rigorous DMF washes and digestion closely matches the amount of cross-linked dotpdc^{4-} present before thermolysis. This clearly demonstrates that the cross-linked ligand dimers were fully incorporated in the framework. Any dangling ligands would have been washed away after cross-linker cleavage, leading to lower-than-expected amounts of H_4dotpdc-COOH.

While the PXRD pattern reveals no loss in crystallinity post-thermolysis (Figure 4b), Mg_2dotpdc-(t)-COOH-49% does not display the expected increase in surface area (Figure 4c, Table S2). Given the known sensitivity of Mg_2dotpdc toward acidic conditions,[46] we hypothesized that the framework may be incompatible with such a high density of free carboxylic acid sites and that higher surface areas may be observed at a lower functional group concentrations. Indeed, at lower concentrations of templated carboxylic acid (<25%), the thermolyzed framework appears pristine by both PXRD and gas sorption studies (Figure 4). After thermolysis, dramatic increases in both the BET and Langmuir surface areas are observed for Mg_2dotpdc-(t)-COOH-23%, from 2290 to 2510 m^2/g and 3660 to 4480 m^2/g, respectively (Figure 4c). Infrared spectroscopy shows a shift in the $\nu_{C=O}$ of the ester linkage from 1705 to 1675 cm^{-1}, consistent with the conversion of the ester to a free carboxylic acid (Figure S20). To our knowledge, this represents the first time that a thermolabile protecting group has been used to install free carboxylic acids within MOF pores. More broadly, this work illustrates how molecular templating can serve as a new and complementary strategy for manipulating the interior surface chemistry of metal−organic frameworks.

CONCLUSION

We have shown that simple, thermolabile tertiary ester-based cross-linkers can be used to template carboxylic acid pairs within metal−organic frameworks. A key advantage of this strategy is how it couples structural versatility with molecular precision. By changing the cross-linker length and geometry, as well as the overall framework topology, it should be possible to precisely fine-tune the ultimate orientation and position of free carboxylic acids within the framework pores. Future studies will investigate whether our templated carboxylic acid pairs can mimic biological active sites, such as the diacid active site of glycosidase[47−49] or the site-isolated carboxylate-bridged diiron sites found in many metalloproteins.[50−52]

ASSOCIATED CONTENT

Supporting Information

The Supporting Information is available free of charge at https://pubs.acs.org/doi/10.1021/jacs.1c04030.

Additional experimental details, ligand syntheses, powder X-ray diffraction data, NMR data, FTIR data, computational details, and gas adsorption data and analysis (PDF)

AUTHOR INFORMATION

Corresponding Author

Dianne J. Xiao − *Department of Chemistry, University of Washington, Seattle, Washington 98195-1700, United States;* orcid.org/0000-0002-5623-9585; Email: djxiao@uw.edu

Authors

Jackson Geary − *Department of Chemistry, University of Washington, Seattle, Washington 98195-1700, United States;* orcid.org/0000-0003-3489-2716

Andy H. Wong − *Department of Chemistry, University of Washington, Seattle, Washington 98195-1700, United States*

Complete contact information is available at: https://pubs.acs.org/10.1021/jacs.1c04030

Notes

The authors declare no competing financial interest.

ACKNOWLEDGMENTS

We gratefully acknowledge University of Washington startup funds and the Donors of the American Chemical Society Petroleum Research Fund for support of this research under PRF# 61949-DNI3. We thank the Mary Gates research scholarship for supporting A.H.W. Part of this work was conducted at the Molecular Analysis Facility, a National Nanotechnology Coordinated Infrastructure (NNCI) site at the University of Washington, which is supported in part by funds from the National Science Foundation (Awards NNCI-2025489, NNCI-1542101), the Molecular Engineering & Sciences Institute, and the Clean Energy Institute. In addition, the authors acknowledge the use of facilities and instrumentation supported by the U.S. National Science Foundation through the UW Molecular Engineering Materials Center (MEM-C), a Materials Research Science and Engineering Center (DMR171797). This work was facilitated through the use of advanced computational, storage, and networking infrastructure provided by the Hyak supercomputer system at the University of Washington.

REFERENCES

(1) Warshel, A.; Sharma, P. K.; Kato, M.; Xiang, Y.; Liu, H.; Olsson, M. H. M. Electrostatic Basis for Enzyme Catalysis. *Chem. Rev.* **2006**, *106* (8), 3210−3235.

(2) Frey, P. A.; Hegeman, A. D. Enzymes and Catalytic Mechanisms. In *Enzymatic reaction mechanisms*; Oxford University Press: Oxford, New York, 2007; pp 1−68.

(3) Knowles, R. R.; Jacobsen, E. N. Attractive Noncovalent Interactions in Asymmetric Catalysis: Links between Enzymes and Small Molecule Catalysts. *Proc. Natl. Acad. Sci. U. S. A.* **2010**, *107* (48), 20678−20685.

(4) Rakowski DuBois, M.; DuBois, D. L. The Roles of the First and Second Coordination Spheres in the Design of Molecular Catalysts

for H_2 Production and Oxidation. *Chem. Soc. Rev.* **2009**, *38* (1), 62−72.
(5) Shook, R. L.; Borovik, A. S. Role of the Secondary Coordination Sphere in Metal-Mediated Dioxygen Activation. *Inorg. Chem.* **2010**, *49* (8), 3646−3660.
(6) Zhao, M.; Wang, H.-B.; Ji, L.-N.; Mao, Z.-W. Insights into Metalloenzyme Microenvironments: Biomimetic Metal Complexes with a Functional Second Coordination Sphere. *Chem. Soc. Rev.* **2013**, *42* (21), 8360.
(7) Visser, S. P. Second-Coordination Sphere Effects on Selectivity and Specificity of Heme and Nonheme Iron Enzymes. *Chem. - Eur. J.* **2020**, *26* (24), 5308−5327.
(8) Dudev, T.; Lim, C. Metal Binding Affinity and Selectivity in Metalloproteins: Insights from Computational Studies. *Annu. Rev. Biophys.* **2008**, *37* (1), 97−116.
(9) Dudev, T.; Lim, C. Competition among Metal Ions for Protein Binding Sites: Determinants of Metal Ion Selectivity in Proteins. *Chem. Rev.* **2014**, *114* (1), 538−556.
(10) Wolfenden, R.; Snider, M. J. The Depth of Chemical Time and the Power of Enzymes as Catalysts. *Acc. Chem. Res.* **2001**, *34* (12), 938−945.
(11) Bour, J. R.; Wright, A. M.; He, X.; Dincă, M. Bioinspired Chemistry at MOF Secondary Building Units. *Chem. Sci.* **2020**, *11* (7), 1728−1737.
(12) Deng, H.; Doonan, C. J.; Furukawa, H.; Ferreira, R. B.; Towne, J.; Knobler, C. B.; Wang, B.; Yaghi, O. M. Multiple Functional Groups of Varying Ratios in Metal-Organic Frameworks. *Science* **2010**, *327* (5967), 846−850.
(13) Kong, X.; Deng, H.; Yan, F.; Kim, J.; Swisher, J. A.; Smit, B.; Yaghi, O. M.; Reimer, J. A. Mapping of Functional Groups in Metal-Organic Frameworks. *Science* **2013**, *341* (6148), 882−885.
(14) Koh, K.; Wong-Foy, A. G.; Matzger, A. J. A Crystalline Mesoporous Coordination Copolymer with High Microporosity. *Angew. Chem., Int. Ed.* **2008**, *47* (4), 677−680.
(15) Furukawa, H.; Ko, N.; Go, Y. B.; Aratani, N.; Choi, S. B.; Choi, E.; Yazaydin, A. O.; Snurr, R. Q.; O'Keeffe, M.; Kim, J.; Yaghi, O. M. Ultrahigh Porosity in Metal-Organic Frameworks. *Science* **2010**, *329* (5990), 424−428.
(16) Koh, K.; Van Oosterhout, J. D.; Roy, S.; Wong-Foy, A. G.; Matzger, A. J. Exceptional Surface Area from Coordination Copolymers Derived from Two Linear Linkers of Differing Lengths. *Chemical Science* **2012**, *3* (8), 2429.
(17) Liu, L.; Konstas, K.; Hill, M. R.; Telfer, S. G. Programmed Pore Architectures in Modular Quaternary Metal−Organic Frameworks. *J. Am. Chem. Soc.* **2013**, *135* (47), 17731−17734.
(18) Yuan, S.; Lu, W.; Chen, Y.-P.; Zhang, Q.; Liu, T.-F.; Feng, D.; Wang, X.; Qin, J.; Zhou, H.-C. Sequential Linker Installation: Precise Placement of Functional Groups in Multivariate Metal−Organic Frameworks. *J. Am. Chem. Soc.* **2015**, *137* (9), 3177−3180.
(19) Yuan, S.; Chen, Y.-P.; Qin, J.-S.; Lu, W.; Zou, L.; Zhang, Q.; Wang, X.; Sun, X.; Zhou, H.-C. Linker Installation: Engineering Pore Environment with Precisely Placed Functionalities in Zirconium MOFs. *J. Am. Chem. Soc.* **2016**, *138* (28), 8912−8919.
(20) Yuan, S.; Zou, L.; Li, H.; Chen, Y.-P.; Qin, J.; Zhang, Q.; Lu, W.; Hall, M. B.; Zhou, H.-C. Flexible Zirconium Metal-Organic Frameworks as Bioinspired Switchable Catalysts. *Angew. Chem., Int. Ed.* **2016**, *55* (36), 10776−10780.
(21) Bosch, M.; Yuan, S.; Rutledge, W.; Zhou, H.-C. Stepwise Synthesis of Metal−Organic Frameworks. *Acc. Chem. Res.* **2017**, *50* (4), 857−865.
(22) Margelefsky, E. L.; Zeidan, R. K.; Davis, M. E. Cooperative Catalysis by Silica-Supported Organic Functional Groups. *Chem. Soc. Rev.* **2008**, *37* (6), 1118.
(23) Chen, L.; Xu, S.; Li, J. Recent Advances in Molecular Imprinting Technology: Current Status, Challenges and Highlighted Applications. *Chem. Soc. Rev.* **2011**, *40* (5), 2922.
(24) Lofgreen, J. E.; Ozin, G. A. Controlling Morphology and Porosity to Improve Performance of Molecularly Imprinted Sol−Gel Silica. *Chem. Soc. Rev.* **2014**, *43* (3), 911−933.
(25) Feng, L.; Wang, K.-Y.; Lv, X.-L.; Powell, J. A.; Yan, T.-H.; Willman, J.; Zhou, H.-C. Imprinted Apportionment of Functional Groups in Multivariate Metal−Organic Frameworks. *J. Am. Chem. Soc.* **2019**, *141* (37), 14524−14529.
(26) Park, K. S.; Ni, Z.; Cote, A. P.; Choi, J. Y.; Huang, R.; Uribe-Romo, F. J.; Chae, H. K.; O'Keeffe, M.; Yaghi, O. M. Exceptional Chemical and Thermal Stability of Zeolitic Imidazolate Frameworks. *Proc. Natl. Acad. Sci. U. S. A.* **2006**, *103* (27), 10186−10191.
(27) Deng, H.; Grunder, S.; Cordova, K. E.; Valente, C.; Furukawa, H.; Hmadeh, M.; Gandara, F.; Whalley, A. C.; Liu, Z.; Asahina, S.; Kazumori, H.; O'Keeffe, M.; Terasaki, O.; Stoddart, J. F.; Yaghi, O. M. Large-Pore Apertures in a Series of Metal-Organic Frameworks. *Science* **2012**, *336* (6084), 1018−1023.
(28) Milner, P. J.; Martell, J. D.; Siegelman, R. L.; Gygi, D.; Weston, S. C.; Long, J. R. Overcoming Double-Step CO_2 Adsorption and Minimizing Water Co-Adsorption in Bulky Diamine-Appended Variants of Mg_2(Dobpdc). *Chem. Sci.* **2018**, *9* (1), 160−174.
(29) Rosi, N. L.; Kim, J.; Eddaoudi, M.; Chen, B.; O'Keeffe, M.; Yaghi, O. M. Rod Packings and Metal−Organic Frameworks Constructed from Rod-Shaped Secondary Building Units. *J. Am. Chem. Soc.* **2005**, *127* (5), 1504−1518.
(30) Xiao, D. J.; Oktawiec, J.; Milner, P. J.; Long, J. R. Pore Environment Effects on Catalytic Cyclohexane Oxidation in Expanded Fe_2(Dobdc) Analogues. *J. Am. Chem. Soc.* **2016**, *138* (43), 14371−14379.
(31) Fracaroli, A. M.; Furukawa, H.; Suzuki, M.; Dodd, M.; Okajima, S.; Gándara, F.; Reimer, J. A.; Yaghi, O. M. Metal−Organic Frameworks with Precisely Designed Interior for Carbon Dioxide Capture in the Presence of Water. *J. Am. Chem. Soc.* **2014**, *136* (25), 8863−8866.
(32) Allen, C. A.; Boissonnault, J. A.; Cirera, J.; Gulland, R.; Paesani, F.; Cohen, S. M. Chemically Crosslinked Isoreticular Metal−Organic Frameworks. *Chem. Commun.* **2013**, *49* (31), 3200.
(33) Allen, C. A.; Cohen, S. M. Exploration of Chemically Cross-Linked Metal−Organic Frameworks. *Inorg. Chem.* **2014**, *53* (13), 7014−7019.
(34) Zhang, Z.; Nguyen, H. T. H.; Miller, S. A.; Cohen, S. M. PolyMOFs: A Class of Interconvertible Polymer-Metal-Organic-Framework Hybrid Materials. *Angew. Chem., Int. Ed.* **2015**, *54* (21), 6152−6157.
(35) Zhang, Z.; Nguyen, H. T. H.; Miller, S. A.; Ploskonka, A. M.; DeCoste, J. B.; Cohen, S. M. Polymer−Metal−Organic Frameworks (PolyMOFs) as Water Tolerant Materials for Selective Carbon Dioxide Separations. *J. Am. Chem. Soc.* **2016**, *138* (3), 920−925.
(36) Ayala, S.; Zhang, Z.; Cohen, S. M. Hierarchical Structure and Porosity in UiO-66 PolyMOFs. *Chem. Commun.* **2017**, *53* (21), 3058−3061.
(37) Schukraft, G. E. M.; Ayala, S.; Dick, B. L.; Cohen, S. M. Isoreticular Expansion of PolyMOFs Achieves High Surface Area Materials. *Chem. Commun.* **2017**, *53* (77), 10684−10687.
(38) MacLeod, M. J.; Johnson, J. A. Block Co-PolyMOFs: Assembly of Polymer−PolyMOF Hybrids via Iterative Exponential Growth and "Click" Chemistry. *Polym. Chem.* **2017**, *8* (31), 4488−4493.
(39) Hurd, C. D.; Blunck, F. H. The Pyrolysis of Esters. *J. Am. Chem. Soc.* **1938**, *60* (10), 2419−2425.
(40) Emovon, E. U.; Maccoll, A. 56. Gas-Phase Eliminations. Part III. The Pyrolysis of Some Secondary and Tertiary Alkyl Acetates. *J. Chem. Soc.* **1962**, 335.
(41) Dugas, V.; Chevalier, Y. Chemical Reactions in Dense Monolayers: In Situ Thermal Cleavage of Grafted Esters for Preparation of Solid Surfaces Functionalized with Carboxylic Acids. *Langmuir* **2011**, *27* (23), 14188−14200.
(42) Healy, C.; Patil, K. M.; Wilson, B. H.; Hermanspahn, L.; Harvey-Reid, N. C.; Howard, B. I.; Kleinjan, C.; Kolien, J.; Payet, F.; Telfer, S. G.; Kruger, P. E.; Bennett, T. D. The Thermal Stability of Metal-Organic Frameworks. *Coord. Chem. Rev.* **2020**, *419*, 213388.
(43) Deshpande, R. K.; Minnaar, J. L.; Telfer, S. G. Thermolabile Groups in Metal-Organic Frameworks: Suppression of Network Interpenetration, Post-Synthetic Cavity Expansion, and Protection of

Reactive Functional Groups. *Angew. Chem., Int. Ed.* **2010**, *49* (27), 4598−4602.
(44) Lun, D. J.; Waterhouse, G. I. N.; Telfer, S. G. A General Thermolabile Protecting Group Strategy for Organocatalytic Metal−Organic Frameworks. *J. Am. Chem. Soc.* **2011**, *133* (15), 5806−5809.
(45) Fracaroli, A. M.; Furukawa, H.; Suzuki, M.; Dodd, M.; Okajima, S.; Gándara, F.; Reimer, J. A.; Yaghi, O. M. Metal-Organic Frameworks with Precisely Designed Interior for Carbon Dioxide Capture in the Presence of Water. *J. Am. Chem. Soc.* **2014**, *136* (25), 8863−8866.
(46) Wang, Z.; Bilegsaikhan, A.; Jerozal, R. T.; Pitt, T. A.; Milner, P. J. Evaluating the Robustness of Metal−Organic Frameworks for Synthetic Chemistry. *ACS Appl. Mater. Interfaces* **2021**, *13* (15), 17517−17531.
(47) Zechel, D. L.; Withers, S. G. Glycosidase Mechanisms: Anatomy of a Finely Tuned Catalyst. *Acc. Chem. Res.* **2000**, *33* (1), 11−18.
(48) Rousseau, C.; Nielsen, N.; Bols, M. An Artificial Enzyme That Catalyzes Hydrolysis of Aryl Glycosides. *Tetrahedron Lett.* **2004**, *45* (47), 8709−8711.
(49) Ortega-Caballero, F.; Rousseau, C.; Christensen, B.; Petersen, T. E.; Bols, M. Remarkable Supramolecular Catalysis of Glycoside Hydrolysis by a Cyclodextrin Cyanohydrin. *J. Am. Chem. Soc.* **2005**, *127* (10), 3238−3239.
(50) Tshuva, E. Y.; Lippard, S. J. Synthetic Models for Non-Heme Carboxylate-Bridged Diiron Metalloproteins: Strategies and Tactics. *Chem. Rev.* **2004**, *104* (2), 987−1012.
(51) Friedle, S.; Reisner, E.; Lippard, S. J. Current Challenges of Modeling Diiron Enzyme Active Sites for Dioxygen Activation by Biomimetic Synthetic Complexes. *Chem. Soc. Rev.* **2010**, *39* (8), 2768.
(52) Jasniewski, A. J.; Que, L. Dioxygen Activation by Nonheme Diiron Enzymes: Diverse Dioxygen Adducts, High-Valent Intermediates, and Related Model Complexes. *Chem. Rev.* **2018**, *118* (5), 2554−2592.

https://doi.org/10.1021/jacs.1c04030
J. Am. Chem. Soc. 2021, 143, 10317−10323